Visual Navigation and Landing Control of an Unmanned Aerial Vehicle on a Moving Autonomous Surface Vehicle via Adaptive Learning

Hai-Tao Zhang [ID], *Senior Member, IEEE*, Bin-Bin Hu, Zhecheng Xu, Zhi Cai, Bin Liu [ID], Xudong Wang, Tao Geng, Sheng Zhong [ID], and Jin Zhao, *Senior Member, IEEE*

Abstract— This article presents a visual navigation and landing control paradigm for an unmanned aerial vehicle (UAV) to land on a moving autonomous surface vehicle (ASV). Therein, an adaptive learning navigation rule with a multilayer nested guidance is designed to pinpoint the position of the ASV and to guide and control the UAV to fulfill horizontal tracking and vertical descending in a narrow landing region of the ASV by means of merely relative position feedback. To ensure the feasibility of the proposed control law, asymptotical stability conditions are derived based on Lyapunov stability theory. Landing experimental results are reported for a UAV-ASV system consisting of an M-100 UAV and a self-developed three-meters-long HUSTER-30 ASV on a lake to substantiate the efficacy of the proposed landing control method.

Index Terms— Adaptive learning, autonomous surface vehicle (ASV), landing, navigation, unmanned aerial vehicle (UAV).

Hai-Tao Zhang, Bin-Bin Hu, and Zhecheng Xu are with the School of Artificial Intelligence and Automation, Huazhong University of Science and Technology, Wuhan 430074, China, also with the Key Laboratory of Image Processing and Intelligent Control, Huazhong University of Science and Technology, Wuhan 430074, China, and also with the State Key Laboratory of Digital Manufacturing Equipment and Technology, Huazhong University of Science and Technology, Wuhan 430074, China (e-mail: zht@mail.hust.edu.cn; hbb@hust.edu.cn; zhechengxu@163.com).

Zhi Cai, Sheng Zhong, and Jin Zhao are with the Key Laboratory of Imaging Processing and Intelligence Control, School of Artificial Intelligence and Automation, Huazhong University of Science and Technology, Wuhan 430074, China (e-mail: caizhi@hust.edu.cn; zs2971@gmail.com; jinzhao617@hust.edu.cn).

Bin Liu and Xudong Wang are with the School of Artificial Intelligence and Automation, Huazhong University of Science and Technology, Wuhan 430074, China, also with the Guangdong HUST Industrial Technology Research Institute, Huazhong University of Science and Technology, Dongguan 523808, China, and also with the Guangdong Province Key Laboratory of Digital Manufacturing Equipment, Huazhong University of Science and Technology, Dongguan 523808, China (e-mail: binliu92@hust.edu.cn; wangxd2016@hust.edu.cn).

Tao Geng is with the Guangdong HUST Industrial Technology Research Institute, Huazhong University of Science and Technology, Dongguan 523808, China, and also with the Guangdong Province Key Laboratory of Digital Manufacturing Equipment, Huazhong University of Science and Technology, Dongguan 523808, China (e-mail: dr.geng@aliyun.com).

Color versions of one or more figures in this article are available at https://doi.org/10.1109/TNNLS.2021.3080980.

Digital Object Identifier 10.1109/TNNLS.2021.3080980

I. INTRODUCTION

IN RECENT years, coordinated motion analysis and control of multiagent systems (MASs) have attracted extensive attentions in the areas of control engineering, systems science, and so on [1]–[5], motivated by the extensive applications of unmanned systems, smart grids, wireless sensor networks, traffic networks, industrial robots, wind farms, etc. The most fascinating feature of MAS collaboration lies in the emergence of high coordination merely via simple protocols of inter-agent interaction, with high efficiency and low cost desirable for numerous applications [6]–[12].

In parallel to the MAS research, the development of unmanned systems also boomed nourished by the significant advances in high-performance integrated circuits and chips, embedded systems, and sensors and actuators. As a representative of unmanned systems, autonomous surface vehicles (ASVs) play a more and more essential role in maritime operations, such as collective resource exploration, environmental monitoring, offshore patrolling, collective rescue, escort, hunting, mine sweeping, and so on [13]–[25]. However, the inherent horizontal 2-D water surface movement areas of multi-ASV groups largely limit their detectable ranges and operational regions. Specifically, for the unreachable areas, like sky and shoals, ASV-borne unmanned aerial vehicles (UAVs) will substantially extend the detectable and operational regions of ASVs from 2-D to 3-D, including maritime-air space survey, reconnaissance, target acquisition, shoal water extraction, and water quality monitoring. Therefore, these years have witnessed the emergence of investigations on UAV-ASV formation cooperation, which are expected to endow the cross-domain groups with high efficiently operational capability in 3-D maritime-air areas.

In the coordination technology of the UAV-ASV system, one of the most challenging issues is the landing of an ASV-borne

UAV to a moving ASV platform. The arduousness of the mission lies in the high precision and efficiency requirements for the anti-wind disturbance control, autonomous navigation, and landing control during all the sequential three steps, i.e., tracking, approaching, and landing. Most of the existing studies were conducted for autonomous navigation and security landing space resolving with the assistance of embedded laser/navigation radars [26], [27] and RGPS [28], [29]. However, such radar-based landing methods require sufficiently large installation space on the UAV and high maintenance cost as well, which hinder their further applications, especially for civil use. Accordingly, it becomes an urgent yet challenging mission to develop a more convenient and less costly autonomous landing scheme to facilitate the cross-domain coordination of UAV-ASV groups.

In this pursuit, with the development of opto-electronic technology, a kind of promising vision-based navigation methods have been intensively explored for UAV-ASV landing. Due to the challenging of motional targets, initial researches focused on a stationary landing platform. As one of the pioneer works, Lin *et al.* [30] designed a monocular camera-based target identification method for a drone. Kim *et al.* [31] developed a guidance-oriented vision processing algorithm, which provides a proper bearing angle for the guidance system. However, with the rapid development of ocean engineering, the existing stationary target landing methods could not fulfill the requirements of the more and more sophisticated water area missions. Hence, more recent efforts have been devoted to the more desirable landing scenarios on motional surface targets. For instance, Serra *et al.* [32] addressed the landing problem on moving platforms via a dynamic image-based visual servo control. Beul *et al.* [33] proposed a camera-based scheme for landing on moving platforms. Tzoumanikas *et al.* [34] designed a visual–inertial estimation-based model predictive controller (MPC) to land a UAV on a moving platform. Baca *et al.* [35] generated a reference trajectory for a UAV to land on a moving car. Rodriguez *et al.* [36] utilized a versatile Gazebo-based reinforcement learning framework to fulfill a continuous UAV landing task. Wu *et al.* [37] designed a dynamic thresholding method for the topological-pattern landmark and took landing experiments on a moving car.

However, the aforementioned studies just focus on ground landing targets (e.g., ground vehicles), which is less challenging than ASV-landing as the latter has unneglectable external disturbances induced by uncertain wind, wave, and tide on water surfaces. Additionally, vision sensor feedback defections induced by vision reflections, vibrations, and bad weathers will even intensify the landing arduousness. Among the few studies on UAVs' landing on water surface vehicles, Lee *et al.* [38] proposed a sliding-mode control scheme for a moving vehicle trajectory tracking and landing. Xia *et al.* [39] addressed a fixed-time control problem of ASV-landing procedures of vertical take-off and landing UAVs suffered by external disturbances. Meng *et al.* [40] proposed a visual/inertial-integrated guidance method for UAV vehicle-board landing. Afterward, Tan *et al.* [41] developed an invariant ellipsoid-based control approach for autonomous vehicle deck landing systems with wind disturbances and measurement noises. Meng *et al.* [42]

designed a vision/radar/inertia navigation system for shipboard landing, where the imbedded camera on the UAV tracks and locks the ASV landmarks to facilitate autonomous landing.

However, due to the practical implementation challenges like wind/wave/tide disturbances, limited sensor range/resolution, surface light reflections, feedback image jittering, and bad weathers, most of the closely-relevant works [38]–[41] still focus on numerical simulation investigation. So far, only a few experimental results [38] of visual navigation precise and secure landing control are conducted with the UAV-ASV cooperation system via only four infrared targets, which could not always guarantee the precise landing of the UAV since the infrared targets are easy to be missed when the UAV-ASV relative height reduces too low. Additionally, sufficiently large landing areas are generally required as well, which is not feasible for small-sized ASVs. Apart from the landing procedure, the capability of autonomous navigation and guidance systems inevitably influences the performance of the landing procedures. Consequently, it becomes an urgent yet challenging mission to propose a niche protocol for guaranteeing autonomous navigation and accurate landing of cross-domain UAV-ASV cooperation systems.

To this end, in this study, a vision-based landing control framework is proposed for a cross-domain autonomous UAV-ASV cooperation equipment composed of an M-100 UAV and a three-meter-long HUSTER-30 ASV located at our testbed lake in Dongguan City, Guangdong Province, China. More precisely, during the landing control procedure, an adaptive learning navigation method is designed with the assistance of a multilayer nested guidance module and a difference GPS device to feedback the position of the ASV, where the UAV could lock the landing area irrelevant of the UAV-ASV height upon detecting any one of the three markers. Moreover, the secure and precise landing could be guaranteed along decreasing height by smoothly switching the makers. Thereby, the UAV fulfills the ASV moving trajectory tracking task via position-feedback regulation governing the UAV-ASV horizontal error to zero. Upon approaching the ASV, with an Adam learning-based landing mark identification and locking procedure, the UAV begins to implement a vision-based horizontal tracking and vertical regulation protocol to land on the moving ASV.

In summary, the contribution of this article is twofold as follows.

1) Proposing an autonomous adaptive learning-based landing control framework for a UAV to land on a moving ASV, which consists of a navigator, an ASV trajectory tracking controller, and a landing height regulator.
2) Establishing a lake-based landing platform consisting of an ASV dock, an M-100 UAV and a three-meter-long HUSTER-30 ASV with a NovAtel-OEM615-typed differential GPS station to substantiate the effectiveness of the proposed control scheme.

The remainder of this article is organized as follows. Section II introduces the preliminaries and the landing control problem for ASV-UAV cooperation systems. Section III proposes a navigation, control, and regulation framework

for a UAV to land on an ASV in motion, and afterward derives the conditions guaranteeing asymptotical stability for the closed-loop system. Extensive landing experiments are conducted to substantiate the effectiveness of the present landing scheme in Section IV. Conclusion is finally drawn in Section V.

II. PROBLEM FORMULATION

Throughout this article, $\mathbb{R}$ and $\mathbb{R}^+$ denote the real number and positive real number, respectively. $\mathbb{R}^n$ denotes the n-dimensional Euclidean space and $\|*\|$ is the Euclidean norm of a vector $*$. e^* denotes exponential power of a square matrix $*$. $*^{-1}$ denotes the inversion of a square matrix $*$. $*^\mathsf{T}$ represents the transpose of a matrix $*$.

Consider an autonomous motional landing system consisting of a UAV and an ASV. In these years, there are significant achievements on the UAV control [43], [44]. Therein, a representative practical method is to simplify a dynamic UAV as a moving particle approximated by the following second-order dynamics in the Cartesian coordinates (see [45], [46])

$$\begin{aligned} \dot{q}(t) &= p(t) \\ \dot{p}(t) &= u(t) \end{aligned} \tag{1}$$

with $q(t) = [q_x, q_y, q_z]^\mathsf{T}$, $p(t) = [p_x, p_y, p_z]^\mathsf{T} \in \mathbb{R}^3$ denoting the position and velocity of the UAV, respectively, and $u(t) = [u_x, u_y, u_z]^\mathsf{T} \in \mathbb{R}^3$ being the control input. Specifically, in the landing scenario, $q_d(t)$ is the center of the ASV landing mark. Meanwhile, a moving ASV with a constant velocity can be regarded as a second-order dynamic with a two-level hierarchical framework, see [18] as

$$\begin{aligned} \dot{q}_d(t) &= p_d(t) \\ \dot{p}_d(t) &= 0 \end{aligned} \tag{2}$$

with $q_d(t) = [q_d^x, q_d^y, q_d^z]^\mathsf{T}$, $p_d(t) = [p_d^x, p_d^y, p_d^z]^\mathsf{T} \in \mathbb{R}^3$ representing the position and velocity of the ASV, respectively.

In real landing procedure of the UAV-ASV system, the ASV position q_d is usually detected by GPS and afterward be transmitted to the UAV, which inevitably introduces positioning inaccuracy due to the inherent GPS measurement error. As a remedy, a landing guidance is thus equipped onboard and identified by a camera embedded in the UAV, which provides a more accurate position feedback of the landing area. However, due to the limited detectable range and resolution, the camera could just catch the guidance with a sufficiently small UAV-ASV distance. Meanwhile, the external disturbances and measurement noises of the ASV like winds, waves, tides, surface reflections, image jittering, and bad weather also influence the identification performance of the landing-oriented guidance module, which thus poses a challenge to access the actual ASV position $q_d(t)$. It is noted that only the position $q_d(t)$ is available to the guidance module and GPS sensors, but not the velocity $p_d(t)$.

Recall the objective of landing UAV on a motional ASV, it is necessary to provide the following two definitions first.

Definition 1 (Horizontal Tracking): A UAV (1) tracks a moving ASV (2) in a horizontal plane with bounded errors
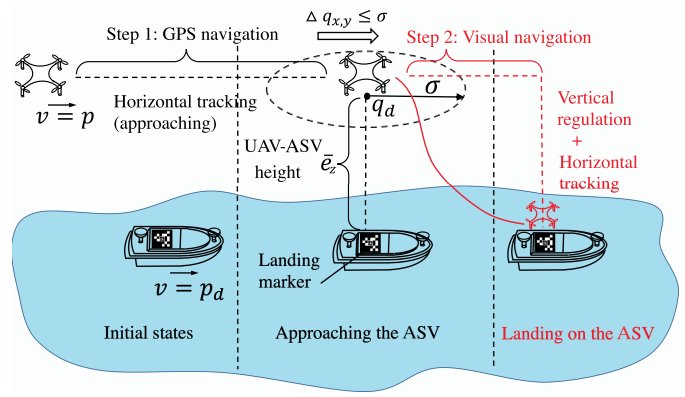

Fig. 1. Two-step landing procedure, step 1: GPS navigation tracking (black trajectory); step 2: Visual navigation landing (red trajectory).

and maintains the initial ASV-UAV relative height if

$$\begin{aligned} \Delta q_x &:= \|q_x(t) - q_d^x(t)\| \le \delta_x \quad \forall t > T \\ \Delta q_y &:= \|q_y(t) - q_d^y(t)\| \le \delta_y \quad \forall t > T \\ \Delta q_z &:= \|q_z(t) - q_d^z(t)\| = \|q_z(0) - q_d^z(0)\| \end{aligned} \tag{3}$$

where $\delta_x, \delta_y \in \mathbb{R}^+$ are the tolerated position errors of the landing area, and $T \in \mathbb{R}^+$ a finite constant time.

Definition 1 describes a practical situation in real landing applications, since the landing time is finite and the landing area for the UAV is just slightly larger than the UAV itself.

Definition 2 (Vertical Regulation): The ASV-UAV relative height settles if

$$\Delta q_z(t) = 0 \quad \forall t > T_z \tag{4}$$

with a finite constant time $T_z \in \mathbb{R}^+$.

The two-step landing procedure is illustrated more vividly in Fig. 1. Therein, with GPS navigation, Step 1 of horizontal tracking (see Definition 1) is conducted by the UAV until the horizontal tracking error

$$\Delta q_{x,y} := \left\| \left[q_x(t) - q_d^x(t), q_y(t) - q_d^y(t) \right]^\mathsf{T} \right\| \le \sigma$$

with a small threshold $\sigma > (\delta_x^2 + \delta_y^2)^{1/2} > 0$. Afterward, with the assistance of adaptive learning-based visual navigation, the ASV landing mark central $q_d(t)$ becomes detectable and lockable by the UAV, and Step 2 of vertical regulation (see Definition 2) is thus triggered together with horizontal tracking for the final touch down.

Now, it is ready to introduce the three main problems addressed in this article as follows.

Problem 1: Design a control law

$$u_{x,y} := f\left(q_x, q_y, p_x, p_y, q_d^x, q_d^y \right)$$

for the UAV of the UAV-ASV system governed by (1) and (2) to fulfill the horizontal tracking mission in Definition 1.

Problem 2: Design an adaptive learning rule to calculate changes for pinpointing the landing position of ASV q_d as

$$q_d := \{\text{2-D visual-guidance barcode, camera}\}$$

for the visual navigation of UAV in the UAV-ASV system.

Problem 3: Design a control law

$$u_z := f\left(q_z, p_z, q_d^z\right)$$

for the UAV of the UAV-ASV system governed by (1) and (2) to achieve the vertical regulation status in Definition 2.

It is noted that, due to the decoupling property of the simplified UAV dynamic in (1), Problems 1 and 3 can be both addressed by separately designing 3-D control signals u_x, u_y, u_z.

III. THEORETICAL RESULTS

In this section, the three parts of the landing control procedure in Fig. 1 will be derived, i.e., horizontal tracking control, adaptive learning-based navigation, and vertical regulation.

A. Horizontal Tracking

We are now ready to propose a tracking control law to tackle Problem 1, i.e., to fulfill Step 1 of the landing procedure in Fig. 1. Before presenting the detailed derivation, a lemma of typical output regulation theory is given first.

Lemma 1 [47]: Consider a linear time-invariant system governed by

$$\dot{x} = \mathcal{A}x + \mathcal{B}u + \mathcal{E}v$$
$$e = \mathcal{C}x + \mathcal{D}u + \mathcal{F}v$$
$$\dot{v} = \mathcal{S}v$$

and a dynamic state feedback controller

$$u = \mathcal{K}_1 x + \mathcal{K}_2 z$$
$$\dot{z} = \mathcal{G}_1 z + \mathcal{G}_2 e$$

where $x \in \mathbb{R}^n, u \in \mathbb{R}^m, e \in \mathbb{R}^p, z \in \mathbb{R}^{n_z}, v \in \mathbb{R}^q$ the system state, input state, regulated output, internal model state, and exosystem signal, respectively and $\mathcal{A} \in \mathbb{R}^{n \times n}, \mathcal{B} \in \mathbb{R}^{n \times m}, \mathcal{C} \in \mathbb{R}^{p \times n}, \mathcal{D} \in \mathbb{R}^{p \times m}, \mathcal{E} \in \mathbb{R}^{n \times q}, \mathcal{F} \in \mathbb{R}^{p \times q}, \mathcal{S} \in \mathbb{R}^{q \times q}, \mathcal{K}_1 \in \mathbb{R}^{m \times n}, \mathcal{K}_2 \in \mathbb{R}^{m \times n_z}, \mathcal{G}_1 \in \mathbb{R}^{n_z \times n_z}, \mathcal{G}_2 \in \mathbb{R}^{n_z \times p}$. Assume $\mathcal{S}$ has no eigenvalue with negative real parts. If $(\mathcal{G}_1, \mathcal{G}_2)$ incorporates a p-copy internal model of $\mathcal{S}$ and the matrix

$$\mathcal{A}_c = \begin{bmatrix} \mathcal{A} + \mathcal{B}\mathcal{K}_1 & \mathcal{B}\mathcal{K}_2 \\ \mathcal{G}_2(\mathcal{C} + \mathcal{D}\mathcal{K}_1) & \mathcal{G}_1 + \mathcal{G}_2\mathcal{D}\mathcal{K}_2 \end{bmatrix}$$

is Hurwitz, then the following Sylvester matrix equation has a unique solution $\mathcal{X} \in \mathbb{R}^{n \times q}, \mathcal{Z} \in \mathbb{R}^{n_z \times q}$ as

$$\mathcal{X}_c \mathcal{S} = \mathcal{A}_c \mathcal{X}_c + \mathcal{B}_c$$
$$\mathbf{0} = \mathcal{C}_c \mathcal{X}_c + \mathcal{D}_c$$

with

$$\mathcal{X}_c = \begin{bmatrix} \mathcal{X} \\ \mathcal{Z} \end{bmatrix}, \quad \mathcal{B}_c = \begin{bmatrix} \mathcal{E} \\ \mathcal{G}_2 \mathcal{F} \end{bmatrix}, \quad \mathcal{C}_c = \begin{bmatrix} \mathcal{C} & \mathcal{D} \end{bmatrix}, \quad \mathcal{D}_c = \begin{bmatrix} \mathcal{F} \end{bmatrix}.$$

To achieve horizontal tracking, it suffices to consider the horizontal plane dynamics of the UAV-ASV system as

$$\dot{\overline{q}}(t) = \overline{p}(t)$$
$$\dot{\overline{p}}(t) = \overline{u}(t) \tag{5}$$

with $\overline{q}(t) = [q_x, q_y]^{\mathsf{T}}, \overline{p} = [p_x, p_y]^{\mathsf{T}}, u(t) = [u_x, u_y]^{\mathsf{T}} \in \mathbb{R}^2$, and

$$\dot{\overline{q}}_d(t) = \overline{p}_d(t)$$
$$\dot{\overline{p}}_d(t) = 0 \tag{6}$$

with $\overline{q}_d(t) := [q_d^x, q_d^y]^{\mathsf{T}}, \overline{p}_d := [p_d^x, p_d^y]^{\mathsf{T}} \in \mathbb{R}^2$. Note that, in Step 1 of the landing procedure, ASV position q_d is just roughly detected by a differential NovAtel-OEM615-typed GPS with ± 0.4 m error, which however suffices the horizontal tracking.

Define the horizontal plane position error between the UAV and the ASV as follows:

$$\overline{e}(t) := \overline{q}(t) - \overline{q}_d(t). \tag{7}$$

It follows from (5) and (6) that

$$\dot{\overline{e}}(t) = \overline{p}(t) - \overline{p}_d(t). \tag{8}$$

A control law for (5) in the horizontal plane is thus designed as

$$\overline{u} = -\begin{bmatrix} k_1 & k_2 \end{bmatrix} \cdot \overline{\xi} - \begin{bmatrix} k_3 & k_4 \end{bmatrix} \cdot \widehat{\xi}$$
$$\dot{\widehat{\xi}} = G_1 \widehat{\xi} + G_2 \overline{e} \tag{9}$$

where $\overline{\xi} := [\overline{q}, \ \overline{p}]^{\mathsf{T}}, \widehat{\xi} := [\widehat{q}, \ \widehat{p}]^{\mathsf{T}} \in \mathbb{R}^2$ are the states of the designed internal model, and $k_1, k_2, k_3, k_4 \in \mathbb{R}^+$ are the control gains to be specified afterward, and

$$G_1 = \begin{bmatrix} 0 & 1 \\ 0 & 0 \end{bmatrix}, \quad G_2 = \begin{bmatrix} 0 \\ 1 \end{bmatrix}. \tag{10}$$

Now, we are ready to present the main technical result concerning Problem 1 as follows.

Theorem 1: The closed-loop system composed of (5)–(7) and (9) is able to achieve the horizontal tracking status in Problem 1, if $k_1, k_2, k_3, k_4 \in \mathbb{R}^+$ satisfy

$$k_2 k_1 - k_4 > 0$$
$$(k_2 k_1 - k_4) k_4 - k_2^2 k_3 > 0. \tag{11}$$

Proof: Substituting $\overline{u}$ in (9) into (5) yields a compact form of (5) as

$$\dot{\overline{\xi}} = A\overline{\xi} + B\widehat{\xi} \tag{12}$$

with

$$A = \begin{bmatrix} 0 & 1 \\ -k_1 & -k_2 \end{bmatrix}, \quad B = \begin{bmatrix} 0 & 0 \\ -k_3 & -k_4 \end{bmatrix}. \tag{13}$$

Analogously, define $\overline{\xi}_d := [\overline{q}_d, \ \overline{p}_d]^{\mathsf{T}}$, one has the horizontal plane dynamic equation of the ASV in (6) as

$$\dot{\overline{\xi}}_d = S\overline{\xi}_d \tag{14}$$

with

$$S = \begin{bmatrix} 0 & 1 \\ 0 & 0 \end{bmatrix}.$$

Then, $\overline{e}$ can be rewritten via $\overline{\xi}, \overline{\xi}_d$ as

$$\overline{e}(t) = C\overline{\xi} + D\overline{\xi}_d \tag{15}$$

with

$$C = \begin{bmatrix} 1 & 0 \end{bmatrix}, \quad D = \begin{bmatrix} -1 & 0 \end{bmatrix}. \tag{16}$$

Let $\varsigma = [\overline{\widetilde{\xi}}, \ \widehat{\widetilde{\xi}}]^{\mathsf{T}}$, it follows from (9), (12), (15) that the regulation system becomes

$$\begin{aligned} \dot{\varsigma} &= A_c \varsigma + B_c \overline{\widetilde{\xi}}_d \\ \dot{\overline{\widetilde{\xi}}}_d &= S \overline{\widetilde{\xi}}_d \\ \overline{e} &= C_c \varsigma + D \overline{\widetilde{\xi}}_d \end{aligned} \tag{17}$$

with

$$A_c = \begin{bmatrix} A & B \\ G_2 C & G_1 \end{bmatrix}, \quad B_c = \begin{bmatrix} 0 \\ G_2 D \end{bmatrix}, \quad C_c = \begin{bmatrix} C & 0 \end{bmatrix}.$$

Due to the minimum characteristic polynomial of matrix $\lambda(S) = \lambda^2$, one has that G_1, G_2 incorporate a p-copy internal model of matrix S in (14) [47]. Moreover, with A, B, G_1, G_2, C defined in (10), (13), (16), it can be derived that

$$A_c = \begin{bmatrix} 0 & 1 & 0 & 0 \\ -k_1 & -k_2 & -k_3 & -k_4 \\ 0 & 0 & 0 & 1 \\ 1 & 0 & 0 & 0 \end{bmatrix} \tag{18}$$

which can be rewritten as a controllable canonical form [48]

$$\overline{A}_c = \begin{bmatrix} 0 & 1 & 0 & 0 \\ 0 & 0 & 1 & 0 \\ 0 & 0 & 0 & 1 \\ -k_3 & -k_4 & -k_1 & -k_2 \end{bmatrix}. \tag{19}$$

With the assistance of Routh stability criterion [49], the matrix $\overline{A}_c$ is Hurwitz if $k_1, k_2, k_3, k_4 \in \mathbb{R}^+$ satisfy

$$k_2 k_1 - k_4 > 0, \ (k_2 k_1 - k_4) k_4 - k_2^2 k_3 > 0 \tag{20}$$

which implies that A_c is Hurwitz as well. According to Lemma 1, one has that the regulation equation of (17) has a solution Σ as

$$\begin{aligned} \Sigma S &= A_c \Sigma + B_c, \\ 0 &= C_c \Sigma + D. \end{aligned} \tag{21}$$

Define $\widetilde{\varsigma} := \varsigma - \Sigma \overline{\widetilde{\xi}}_d$ as the state errors, the temporal derivative of $\widetilde{\varsigma}$ along the trajectories of (17) and (21) writes

$$\begin{aligned} \dot{\widetilde{\varsigma}} &= A_c \varsigma + B_c \overline{\widetilde{\xi}}_d - \Sigma S \overline{\widetilde{\xi}}_d \\ &= A_c \widetilde{\varsigma} + (A_c \Sigma + B_c - \Sigma S) \overline{\widetilde{\xi}}_d \\ &= A_c \widetilde{\varsigma} \end{aligned} \tag{22}$$

which implies that $\lim_{t \to \infty} \widetilde{\varsigma}(t) = 0$ exponentially due to the Hurwitz matrix A_c. On the other hand, considering (21), it can be derived that

$$\begin{aligned} \overline{e} &= C_c \varsigma + D \overline{\widetilde{\xi}}_d \\ &= C_c \widetilde{\varsigma} + C_c \Sigma \overline{\widetilde{\xi}}_d + D \overline{\widetilde{\xi}}_d \\ &= C_c \widetilde{\varsigma} \end{aligned} \tag{23}$$

which implies that $\lim_{t \to \infty} \overline{e}(t) = 0$ exponentially if $\lim_{t \to \infty} \widetilde{\varsigma}(t) = 0$. Then, it derives that these exists a finite time $T_1 \in \mathbb{R}^+$ such that $\Delta q_x(t) \le \delta_x$ and $\Delta q_y(t) \le \delta_y, \forall t > T_1$, i.e., Problem 1 is solved. The proof is thus completed. $\square$
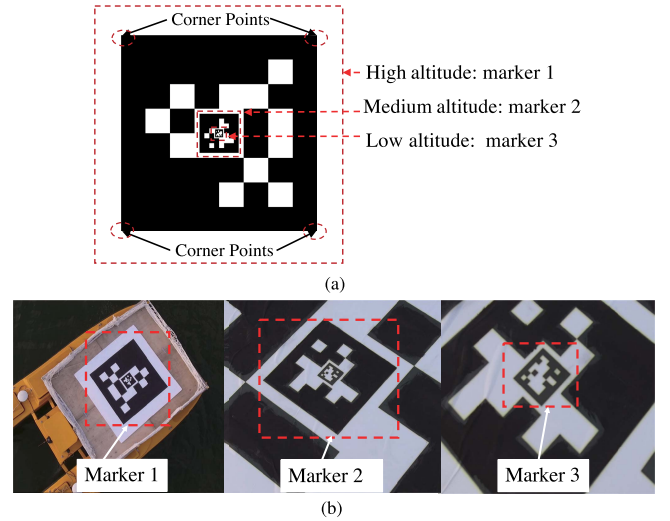

Fig. 2. (a) Multilayer nested 2-D barcode consisting of high-, medium-, and low-altitude markers. (b) Different-size guidance recognition during the landing process.

Remark 1: The proposed $\widehat{\widetilde{\xi}}$ in (9) is designed based on an internal model principle (IMP) [47], which tracks the moving ASV merely with rough GPS position feedback signal q_d. Moreover, IMP substantially eliminates the influence of external disturbances on the UAV like winds and surface light reflects, which endows the controller (9) with desirable robustness in real landing applications.

Remark 2: For the low speed ASV tracking scenario, the UAV tackles Problem 1 with a low frequency, which thus implies the dynamic matrix G_1 in (10) can be ignored as 0. In accordance, the internal model $\widehat{\widetilde{\xi}}$ can be simplified as $\dot{\widehat{\widetilde{\xi}}} = G_2 \overline{e}$, which simplifies the control law (9) into

$$\overline{u} = -\begin{bmatrix} k_1 & k_2 \end{bmatrix} \cdot \overline{\widetilde{\xi}} - \begin{bmatrix} k_3 & k_4 \end{bmatrix} \int G_2 \overline{e}(s) ds. \tag{24}$$

In this way, the output regulation controller (9) is simplified to a proportional-integral (PI) form, which facilitates the control parameters turning in real UAV-ASV landing applications.

B. Learning-Based Navigation

To fulfill the high-precision visual navigation mission, i.e., Step 2, of the landing procedure in Fig. 1, Problem 2 should be addressed first. To this end, a guidance 2-D barcode as show in Fig. 2(a), namely AprilTag2 [50], i.e., an $80 \times 80 \ \text{cm}^2$ rectangle containing multilayer nested block information will be identified by the onboard DJI Zenmuse Z3 camera of the UAV. More precisely, as show in Fig. 2(b), the side length of marker 2 (medium altitude: 1.2–5 m) is 1/5 of that of marker 1 (high altitude: 5–15 m), and so does the side length proportion of marker 3 (low altitude: ≤ 1.2 m) to marker 2. In this way, the precise landing position can be locked along by smoothly switching the makers when reducing UAV-ASV relative height $\overline{e}_z$.

During the visual navigation, the UAV camera firstly detects the rectangle of the 2-D barcode in Fig. 2 with an edge detection approach. Afterward, the UAV is to judge whether
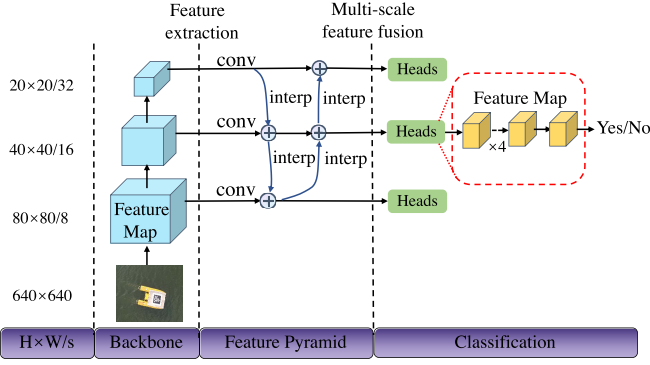
Fig. 3. Architecture of the adaptive learning-based CNN, where the matrix block represents the feature map, H and W are the height and width of feature map, respectively. "$/s$" ($s = 8, 16, 32$) denotes the down-sampling ratio of the feature maps at the level to the input image. "Conv" and "interp" denote the convolution and the bilinear interpolation, respectively. "Heads" represents a general name of several convolutions after feature fusion. "$\times 4$" represents convolution four times.

the rectangle is the landing marker. Different from a typical image segmentation method, an adaptive learning-based convolution neural network (CNN) is proposed to fulfill the real-time requirement of UAV-ASV landing (see [51]), which consists of a backbone network, a feature pyramid, and a classification layer with an Adam learning algorithm in Fig. 3. The number of training and validation pictures are 1532 and 383, respectively, where the accuracies of the proposed CNN in training and validation data are given as 99.4% and 98.3%, respectively.

To train the parameters $\omega \in \mathbb{R}^v$ in the proposed CNN, a cost function containing the training error is given as follows:

$$E(\omega) = \sum_{i=1}^{P} \sum_{j=1}^{N_L} \left(o_{j,i}^L - y_{j,i} \right)^2 \tag{25}$$

where P is the number of patterns of the marker from different angle perspectives, N_L is the number of neurons in output layer, $o_{j,i}^L$ is the output of neuron j in the ith pattern, and $y_{j,i}$ is the target in the ith pattern.

Then, the Adam learning algorithm [52] is utilized to minimize $E(\omega)$ in (25). To this end, define $g_t := \nabla_\omega E(\omega)$, one has

$$\omega_t = \omega_{t-1} - \frac{\alpha}{\sqrt{\widehat{n}_t} + \epsilon} \widehat{m}_t \tag{26}$$

with a constant parameter $\epsilon \in \mathbb{R}^+$, $\alpha \in \mathbb{R}^+$ is the step size, and bias-corrected estimates $\widehat{m}_t, \widehat{n}_t$ are derived as

$$
\begin{aligned}
\widehat{m}_t &= \frac{m_t}{1 - \beta_1^t} \\
\widehat{n}_t &= \frac{n_t}{1 - \beta_2^t} \\
m_t &= \beta_1 m_{t-1} + (1 - \beta_1) g_t \\
n_t &= \beta_2 n_{t-1} + (1 - \beta_2) g_t^2
\end{aligned}
$$

with moving averages of the gradient m_t, squared gradient n_t, and parameters $\beta_1, \beta_2, \beta_1^t, \beta_2^t \in [0, 1)$.

With the identified marker, the essential four corners of the 2-D barcode are calculated as a pixel $\mu_i = [\eta_i, \omega_i, 1]^\mathsf{T}$,

$i = 1, 2, 3, 4$ for visual navigation, where η_i and ω_i denote the horizontal and vertical coordinate, respectively. More precisely, define the corner positions in the camera coordinate as $\overline{\varsigma}_i := [\overline{X}_i, \overline{Y}_i, \overline{Z}_i]^\mathsf{T} \in \mathbb{R}^3$, thus the relationship between μ_i and $\overline{\varsigma}_i$ can be formulated as [53]

$$\overline{Z}_i \mu_i = \mathbf{K} \overline{\varsigma}_i \tag{27}$$

with the camera intrinsics matrix

$$\mathbf{K} = \begin{bmatrix} f_x & 0 & c_x \\ 0 & f_y & c_y \\ 0 & 0 & 1 \end{bmatrix} \tag{28}$$

and constants f_x, f_y, c_x, c_y.

Define the corner positions in earth coordinate as $\varsigma_i := [X_i, Y_i, Z_i]^\mathsf{T} \in \mathbb{R}^3$, then the relationship between $\overline{\varsigma}_i$ and ς_i becomes

$$\overline{\varsigma}_i = \mathbf{R} \varsigma_i + \varphi \tag{29}$$

where $\mathbf{R} \in \mathbb{R}^{3 \times 3}$ and $\varphi \in \mathbb{R}^{3 \times 1}$ are the rotation and the translation matrices from earth coordinate to camera coordinate, respectively. It follows from (27) and (29) that the coordinate transformation from 3-D to 2-D coordinate writes

$$\overline{Z}_i \mu_i = \mathbf{K}(\mathbf{R} \varsigma_i + \varphi). \tag{30}$$

Design a cost function of the re-projection error of the four corners as

$$V(\mathbf{R}, \varphi) = \frac{1}{2} \sum_{i=1}^{4} \left\| \mu_i - \frac{1}{\overline{Z}_i} \mathbf{K}(\mathbf{R} \varsigma_i + \varphi) \right\|^2. \tag{31}$$

According to Lie algebra [54], it is noted that $\mathbf{R} \varsigma_i = e^{\psi(\chi)} \varsigma_i$, where $\psi(\cdot) : \mathbb{R}^3 \to \mathbb{R}^{3 \times 3}$ is a function with an input vector $\chi = [\chi_1, \chi_2, \chi_3]^\mathsf{T} \in \mathbb{R}^3$ as

$$\psi(\chi) = \begin{bmatrix} 0 & -\chi_3 & \chi_2 \\ \chi_3 & 0 & -\chi_1 \\ -\chi_2 & \chi_1 & 0 \end{bmatrix}. \tag{32}$$

Then, the index (31) is rewritten as an unconstrained optimization index

$$V(\chi, \varphi) = \frac{1}{2} \sum_{i=1}^{4} \left\| \mu_i - \frac{1}{\overline{Z}_i} \mathbf{K}\left(e^{\psi(\chi)} \varsigma_i + \varphi\right) \right\|^2. \tag{33}$$

To facilitate a real-time optimization with (33) in the typical Perspective-n-Points (PnP) problem, a neurodynamic optimization method [55], [56] is utilized as

$$\epsilon \frac{d}{dt}(\chi, \varphi) = -\nabla_{(\chi, \varphi)} V(\chi, \varphi) \tag{34}$$

with $\epsilon \in \mathbb{R}^+$ a time constant. It is noted that the convergence time of the optimal solution in (34) is proportional to ϵ. To this end, $(\chi^*, \varphi^*) = \arg \min_{\chi, \varphi} V(\chi, \varphi)$ can be attained.

With the optimized χ^*, φ^* yielded, $\mathbf{R}$ and φ can be calculated as

$$\mathbf{R} = e^{\psi(\chi^*)}, \quad \varphi = \varphi^*. \tag{35}$$

Define the position in the camera homogeneous coordinate as $\overline{\tau}_c := [0, 0, 0, 1]^\mathsf{T}$, the relative position

$\widetilde{\tau}_c = [\widetilde{X}_c, \widetilde{Y}_c, \widetilde{Z}_c, 1] \in \mathbb{R}^4$ between the camera and the ASV in the world homogeneous coordinate is calculates as

$$\widetilde{\tau}_c = \mathbf{T}^{-1}\overline{\tau}_c \qquad (36)$$

with a coordinate transformation matrix

$$T = \begin{bmatrix} \mathbf{R} & \varphi \\ \mathbf{0}^\top & 1 \end{bmatrix} \in \mathbb{R}^{4\times 4}. \qquad (37)$$

It implies the relative position $\overline{\tau}_c = [\widetilde{X}_c, \widetilde{Y}_c, \widetilde{Z}_c] \in \mathbb{R}^3$ in the world coordinate. Combined with the position $q(t)$ captured by the onboard GPS of M-100 UAV, the accurate position of the target $q_d = \overline{\tau}_c + q$ is derived according to an Adam-based navigation algorithm summarized in Algorithm 1. Along the decreased UAV height during the landing procedure, the high-, medium-, and low-altitude 2-D barcode markers in Fig. 2 can be identified and locked for accurate vision guidance to realize Step 2 of the landing procedure in Fig. 1. The merit of the proposed Algorithm 1 lies in its high computational efficiency and nonstationary optimization capability with noisy gradients induced by the vibrations of the UAV and the ASV moving in the windy and wavy water area.

Algorithm 1 Adam Adaptive Learning-Based Navigation Algorithm

---

Step 1: Detect the rectangle of the marker in Fig. 2 (a) with an edge detection approach;
Step 2: Identify the marker and four corner positions μ_i in Fig. 2 (a) by using an Adam learning-based CNN structure;
Step 3: Calculate $\mathbf{R} = e^{\psi(\chi^*)}, \varphi = \varphi^*$ in (35) in the PnP problem via a neurodynamic optimization method;
Step 4: Pinpoint the position $q_d = \overline{\tau}_c + q$ with position q captured by the onboard GPS of M-100 UAV.

Remark 3: In previous visual navigation methods [40], [42], only four infrared targets are equipped on the platform. These schemes could not always guarantee the precise landing of the UAV since the infrared targets could be missed when the UAV-ASV relative height reduces too low (less than 1.2 m for example). Additionally, it usually requires large landing area, which is not feasible for small-sized ASVs like the present case. As a remedy, the present study designs multilayer nested markers instead, the UAV could lock the landing area irrelevant of the UAV-ASV height once detecting any one marker of the three markers in Fig. 2. In this way, secure and precise landing could be guaranteed along decreasing height by smoothly switching the makers. Therefore, the proposed algorithm is more accurate, effective, and secure compared with [40], [42]. ∎

C. Vertical Regulation

Upon completing Step 1 of the landing procedure in Fig. 1, one has $\lim_{t\to\infty} \overline{e}(t) = 0$ in accordance to Theorem 1. In other words, for any prescribed bound $\sigma \in \mathbb{R}^+$, there exists a time period $T_p > 0$ such that $\|e(t)\| \leq \sigma$ if $t > T_p$. Afterward, we can address the vertical regulation in Problem 3 with the visually identified landing position p_d resulted from Algorithm 1.

Unlike subsection III-A, only longitudinal-axis dynamic of the UAV-ASV system is considered in Problem 3 due to the decoupling property of the simplified UAV dynamic, which are formulated as

$$\dot{q}_z(t) = p_z(t)$$
$$\dot{p}_z(t) = u_z(t) \qquad (38)$$

and

$$\dot{q}_d^z(t) = p_d^z(t)$$
$$\dot{p}_d^z(t) = 0 \qquad (39)$$

by virtue of (1) and (2). Let $\overline{e}_z$ be the relative UAV-ASV height shown in Fig. 1 as

$$\overline{e}_z = q_z - q_d^z. \qquad (40)$$

It then follows from (38) and (39) that

$$\dot{\overline{e}}_z = p_z - \dot{q}_d^z. \qquad (41)$$

A control law to achieve vertical regulation is thus designed as follows:

$$u_z = -k_5\dot{\overline{e}}_z - k_6(k_5\overline{e}_z + p_z - \dot{q}_d^z) + \ddot{q}_d^z \qquad (42)$$

where $k_5, k_6 \in \mathbb{R}^+$ are the control gains to be specified afterward. Now, we are ready to present the main technical result concerning Problem 3 as below.

Theorem 2: The closed-loop system composed of (38), (39) and (42) is able to achieve the relative vertical regulation in Problem 3.

Proof: We first denote h_z as a desired height

$$h_z = k_5\overline{e}_z + p_z - \dot{q}_d^z. \qquad (43)$$

Using the fact that $p_z - \dot{q}_d^z = h_z - k_5\overline{e}_z$, it follows from (41) that

$$\dot{\overline{e}}_z = -k_5\overline{e}_z + h_z. \qquad (44)$$

Let a Lyapunov function candidate be

$$V_2(\overline{e}_z) = \frac{1}{2}\overline{e}_z^2. \qquad (45)$$

Its time derivative of $V_2(\overline{e}_z)$ along the trajectories of (44) is

$$\begin{aligned}
\dot{V}_2(\overline{e}_z) &= \overline{e}_z\dot{\overline{e}}_z \\
&= \overline{e}_z(-k_5\overline{e}_z + h_z) \\
&\leq -k_5(1-c_2)\overline{e}_z^2 + |\overline{e}_z|(|h_z| - k_5c_2|\overline{e}_z|) \\
&\leq 0 \qquad (46)
\end{aligned}$$

with $c_2 \in (0, 1)$. Then, one has $\dot{V}_2(\overline{e}_z) \leq -k_5(1-c_2)\overline{e}_z^2, \forall|\overline{e}_z| \geq |h_z|/(c_2k_5)$. If $|\overline{e}_z(0)| \geq |h_z|/(c_2k_5)$, then $\dot{V}_2(\overline{e}_z) \leq 0$, which implies that $|\overline{e}_z|$ converges into the ball of radius $|h_z|/(c_2k_5)$. If $|\overline{e}_z(0)| < |h_z|/(c_2k_5)$. It is clear that $|\overline{e}_z(0)|$ has already been in the ball of radius $|h_z|/(c_2k_5)$. Both cases satisfy the definition of input-to-state stability (ISS) [53], which implies that $|\overline{e}_z(0)|$ could be randomly picked. Accordingly, the closed-loop system (44) is input-to-state stable (ISS) [57] with respect to $|h_z|$ satisfying

$$\overline{e}_z(t) = \beta(|\overline{e}_z(0)|, t) + \kappa_2 \sup_{\tau \geq 0} |h_z(\tau)| \quad \forall t > 0 \qquad (47)$$

where $\kappa_2 = 1/(k_5 c_2)$ is the gain of the system (see [58]). Then, the temporal derivative of h_z along the trajectory of (38) becomes

$$\dot{h}_z = k_5 \dot{\bar{e}}_z + u_z - \ddot{q}_d^z. \tag{48}$$

Substituting the controller (42) into (48) yields

$$\begin{aligned} \dot{h}_z &= k_5 \dot{\bar{e}}_z - k_5 \dot{\bar{e}}_z - k_6 h_z + \ddot{q}_d^z - \ddot{q}_d^z \\ &= -k_6 h_z \end{aligned} \tag{49}$$

which implies that $\lim_{t\to\infty} h_z(t) = 0$, exponentially. It follows from (47) that $\lim_{t\to\infty} \bar{e}_z(t) = 0$, exponentially. Note that $\Delta q_z = \|\bar{e}_z\|$ in virtue of (3) and (40). Analogously, these exists a finite time $T_2 \in \mathbb{R}^+$ and a small constant $\delta_z \in \mathbb{R}^+$ such that $\Delta q_z(t) \le \delta_z, \forall t > T_2$. Afterward, the UAV settles on the landing platform safely (i.e., Problem 3 is solved). The proof is thus completed. $\square$

Remark 4: When the ASV moves at a sufficiently low velocity, the influence of the surfaces waves and tides can be neglected, which implies the ASV moves in a horizontal plane. It can be assumed that q_d^z is a constant, and hence $\dot{q}_d^z = 0, \ddot{q}_d^z = 0$. In such a situation, the control law (42) can be approximated as

$$\begin{aligned} u_z &= -k_5 \dot{\bar{e}}_z - k_6 (k_5 \bar{e}_z + p_z - \dot{q}_d^z) + \ddot{q}_d^z \\ &\approx -(k_5 + k_6) \dot{\bar{e}}_z - k_6 k_5 \bar{e}_z. \end{aligned} \tag{50}$$

In this way, the output control law (9) is simplified in a proportional-differential (PD) form, which facilitates the control parameter turning in landing applications.

IV. EXPERIMENTAL RESULTS

In this section, we elaborate on our experimental platform, setup, and results on the learning-based navigation and landing control on established cross-domain UAV-ASV system located on Songshan Lake, Dongguan, Guangdong, China.

A. UAV-ASV Experimental Platform

As shown in Fig. 4(a), our established UAV-ASV platform consists of a DJI Matrice-100 (M-100) UAV and a HUSTER-30 ASV. The UAV is 65.0 cm long in wheelbase, which is equipped with four rotor modules (DJI 3510), a GPS module (A2 GPS PRO PLUS), a camera (DJI Zenmuse Z3), a 5 g Wi-Fi (VM5g), and a battery (TB47D). All modules are monitored by a control module (MANIFOLD V1). Our developed HUSTER-30 ASV is 300 cm in length, 185 cm in width, and 53 cm in height, which consists of two motor drivers (SEAKING-V3), a battery (RUIYI-200), two antennas (Harxon GPS500), a WiFi (VM5g), an embedded controller (STM32F407VGT6), and a landing platform. It is noted that the landing platform consists of a multilayer nested 2-D barcode (80 cm × 80 cm) in Fig. 2 and a metal frame (180 cm × 120 cm). Table I shows the features of the essential modules in the cross-domain UAV-ASV platform.

As shown in Fig. 4(b), with the VM5g Wi-Fi module embedded on both ASV and UAV, the rough ASV position detected by the GPS module is transferred to the UAV at

TABLE I
MAIN MODULES IN THE UAV-ASV PLATFORM

| Module	Type	Parameters
Rotor	DJI 3510	Rated torque: 0.14Nm, rated speed: 800rpm
GPS	A2 GPS PRO PLUS	Horizontal accuracy: ±2.5m, Vertical accuracy: ±0.5m
Camera	Zenmuse Z3	Image resolution: 4000dpi×3000dpi
Wi-Fi	VM5g	Power: 1.3-3.75w, distance: 700m
Battery	TB47D	Capacity: LiPo 6s, 22.2V, 4500mAh, maximum velocity: 17m/s
Controller	MANIFOLD-V1	Power: 15w, RAM: 2GB, EMMC: 16GB
Driver	SEAKING-V3	Voltage: 5-12s Lipo (21-50.4V), current: 130A
Antenna	Harxon GPS500	Signal reception: GPS, GLONASS, Beidou and L-Band, Gain: 40dB
Battery:	RUIYI-200	Capacity: 54.6V, 120Ah, maximum velocity: 3m/s
Controller	STM32F407VGT6	Flash: 1024kB, frequency: 72M, pin:144
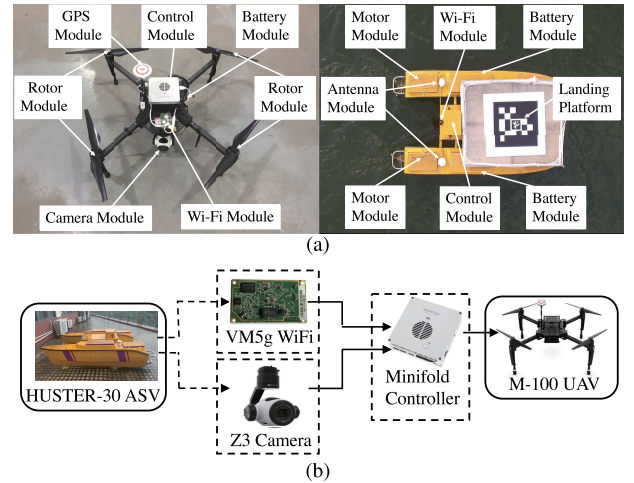
Fig. 4. Our cross-domain UAV-ASV cooperative platform. (a) Components of the UAV-ASV system. (b) Operating procedure of the UAV-ASV system.

a frequency of 1 Hz. Upon catching the ASV, or completing Step 1 in Fig. 1, the UAV-ASV relative displacement is calculated by the Z3 camera with the assistance of the identified precise position p_d of the landing barcode in Fig. 2. Thereafter, with the received distance and landing position, the embedded Minifold V1 controller generates the execution signal to control the rotors to fulfill the landing mission, or Step 2 in Fig. 1. Meanwhile, the status trajectories and the controller parameters are all recorded by the Minifold V1 controller for data analysis.

B. Setup and Results

In the experiment, the parameters of the camera intrinsics $\mathbf{K}$ in (28) are chosen as $f_x = 1048.9125, c_x = 662.2501, f_y = 1045.4800, c_y = 370.6075$. The positions of four corners in the world coordinate are set as $\mathbf{q_1} = [-40, -40, 0]^\top$ cm, $\mathbf{q_2} = [-40, 40, 0]^\top$ cm, $\mathbf{q_3} = [40, 40, 0]^\top$ cm, $\mathbf{q_4} = [40, -40, 0]^\top$ cm. To satisfy the inequality (11), the parameters of the controller (9) are set as $k_1 = 2, k_2 = 2, k_3 = 0.5, k_4 = 1$ for horizontal tracking. In Step 2 of vertical regulation,
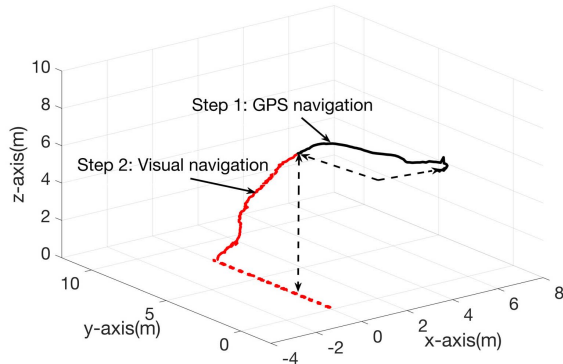
Fig. 5. 3-D view of the detailed UAV-ASV landing process, where the solid black and red curves denote respectively steps 1, and 2 of the UAV, and the dashed red curves denote the trajectories of the ASV.
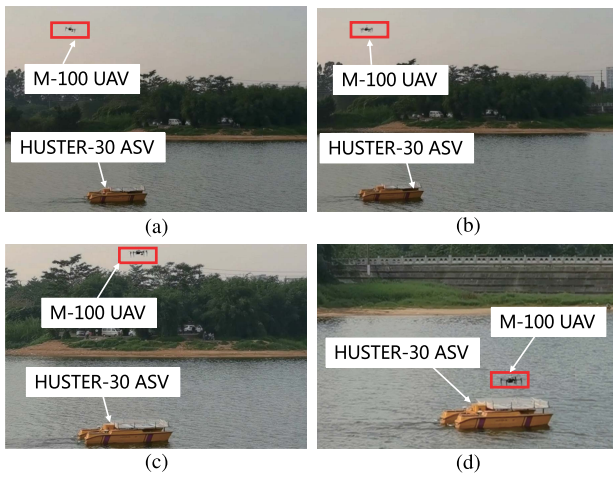

Fig. 6. Four consecutive landing snapshots of the M-100 UAV on a moving HUSTER-30 ASV, where the red rectangle highlights M-100 UAV. (a) Initial positions. (b) Horizontal tracking. (c) Vertical regulation. (d) Landing on the ASV.

the parameters of the controller (42) are set as $k_5 = 1$, $k_6 = 10$. The control signal of (9) and (42) is updated by the embedded controller at a sampling and updating frequency of 20 Hz. As for the HUSTER-30 ASV, the initial position of the HUSTER-30 ASV is randomly set and the velocity of p_d in (2) is regulated as a constant $p_d = [1.2, 0]^\mathsf{T}$ m/s with the two-level controller proposed in [18], [21].

The UAV takes off initially from the lake shore and hovers at a desired height. Fig. 5 shows the landing trajectories of the UAV on a moving ASV with the learning-based vision navigation, where the landing process are separated into Steps 1 and 2 as shown in Fig. 1. To illustrate the landing process more vividly, Fig. 6 shows four consecutive snapshots. Fig. 7 shows that both the relative horizontal position error $\bar{e} = [\bar{e}_x, \bar{e}_y]^\mathsf{T}$ and altitude error $\bar{e}_z$ shrink to zeros in less than 28 seconds. Moreover, It is noted that the M-100 UAV conducts horizontal tracking in only the first nine seconds before driving the relative horizontal position error inside the prescribed threshold $\|\sigma\| \leq 1.5$ m. Afterward, the UAV begins to fulfill the vertical regulation mission illustrated in Fig. 7. As shown in Fig. 2, the three-layer nested 2-D barcode is
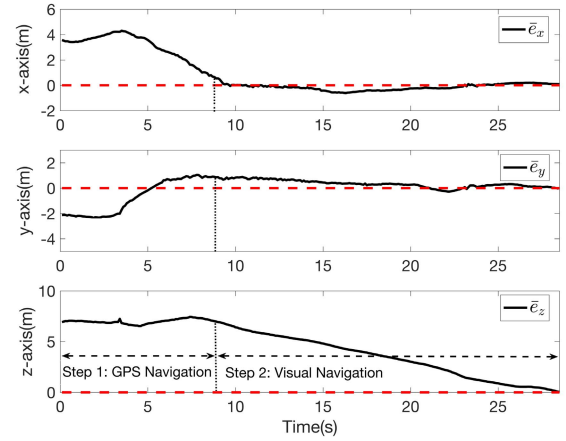

Fig. 7. Transient relative position errors $\bar{e}_x, \bar{e}_y, \bar{e}_z$ toward zeros in the horizontal tracking and vertical regulation.

detected by the Z3 camera, where the visual guidance from large- to medium- and to small-sized markers are identified along decreasing relative UAV-ASV height. The real landing experiments are conducted on the ASV-UAV system as shown in Fig. 6. The feasibility of the proposed relative position feedback control method is thus verified on the UAV-ASV landing mission with horizontal tracking and vertical descending.

V. CONCLUSION

In this article, we present a practical paradigm on the visual navigation and landing control of a UAV to land on a moving ASV with unknown velocity. The proposed landing procedure consists of two consecutive missions; i.e., GPS navigation horizontal tracking and visual navigation vertical/horizontal regulation. We derive the asymptotical stability conditions for the closed-loop UAV-ASV landing system. We also substantiate the effectiveness of the proposed landing scheme with experimental results based on our lake-based platform composed of an M-100 UAV and a self-developed HUSTER-30 ASV. Future work will focus on in-depth theoretical analysis, cohesive system designs, and practical applications of UAV-ASV coordinated systems in complex aquatic environments, such as the distributed landing control of multiUAV on multiple motional ASVs.

REFERENCES

[1] C. W. Reynolds, "Flocks, herds, and schools: A distributed behavioral model," *Comput. Graph.*, vol. 21, no. 4, pp. 25–34, 1987.
[2] R. Olfati-Saber, "Flocking for multi-agent dynamic systems: Algorithms and theory," *IEEE Trans. Autom. Control*, vol. 51, no. 3, pp. 401–420, Mar. 2006.
[3] H.-T. Zhang, C. Zhai, and Z. Chen, "A general alignment repulsion algorithm for flocking of multi-agent systems," *IEEE Trans. Autom. Control*, vol. 56, no. 2, pp. 430–435, Feb. 2011.

[4] X. Mo, Z. Chen, and H.-T. Zhang, "Effects of adding a reverse edge across a stem in a directed acyclic graph," *Automatica*, vol. 103, pp. 254–260, May 2019.

[5] H. Meng, H.-T. Zhang, Z. Wang, and G. Chen, "Event-triggered control for semiglobal robust consensus of a class of nonlinear uncertain multiagent systems," *IEEE Trans. Autom. Control*, vol. 65, no. 4, pp. 1683–1690, Apr. 2020, doi: 10.1109/TAC.2019.2932752.

[6] Z. Chen and H.-T. Zhang, "No-beacon collective circular motion of jointly connected multi-agents," *Automatica*, vol. 47, no. 9, pp. 1929–1937, Sep. 2011.

[7] H.-T. Zhang, Z. Chen, and M.-C. Fan, "Collaborative control of multi-vehicle systems in diverse motion patterns," *IEEE Trans. Control Syst. Technol.*, vol. 24, no. 4, pp. 1488–1494, Jul. 2016.

[8] X. Ge and Q.-L. Han, "Distributed formation control of networked multi-agent systems using a dynamic event-triggered communication mechanism," *IEEE Trans. Ind. Electron.*, vol. 64, no. 10, pp. 8118–8127, Oct. 2017.

[9] G. D. Khan, Z. Chen, and H. Meng, "Output synchronization of nonlinear heterogeneous multi-agent systems with switching networks," *Syst. Control Lett.*, vol. 125, pp. 45–50, Mar. 2019.

[10] P. Liu, Z. Zeng, and J. Wang, "Asymptotic and finite-time cluster synchronization of coupled fractional-order neural networks with time delay," *IEEE Trans. Neural Netw. Learn. Syst.*, vol. 31, no. 11, pp. 4956–4967, Nov. 2020, doi: 10.1109/TNNLS.2019.2962006.

[11] L. Kou, Z. Chen, and J. Xiang, "Cooperative fencing control of multiple vehicles for a moving target with an unknown velocity," *IEEE Trans. Autom. Control*, early access, Apr. 23, 2021, doi: 10.1109/TAC.2021.3075320.

[12] L. Kou, Y. Huang, Z. Chen, S. He, and J. Xiang, "Cooperative fencing control of multiple second-order vehicles for a moving target with and without velocity measurements," *Int. J. Robust Nonlinear Control*, Mar. 2021, doi: 10.1002/rnc.5493.

[13] Z. Peng, J. Wang, and D. Wang, "Containment maneuvering of marine surface vehicles with multiple parameterized paths via spatial-temporal decoupling," *IEEE/ASME Trans. Mechatronics*, vol. 22, no. 2, pp. 1026–1036, Apr. 2017.

[14] Z. Peng, J. Wang, and D. Wang, "Distributed containment maneuvering of multiple marine vessels via neurodynamics-based output feedback," *IEEE Trans. Ind. Electron.*, vol. 64, no. 5, pp. 3831–3839, May 2017.

[15] Z. Peng, J. Wang, and D. Wang, "Distributed maneuvering of autonomous surface vehicles based on neurodynamic optimization and fuzzy approximation," *IEEE Trans. Control Syst. Technol.*, vol. 26, no. 3, pp. 1083–1090, May 2018.

[16] L. Liu, D. Wang, Z. Peng, C. L. P. Chen, and T. Li, "Bounded neural network control for target tracking of underactuated autonomous surface vehicles in the presence of uncertain target dynamics," *IEEE Trans. Neural Netw. Learn. Syst.*, vol. 30, no. 4, pp. 1241–1249, Apr. 2019.

[17] J. Wang, J. Wang, and H. Che, "Task assignment for multivehicle systems based on collaborative neurodynamic optimization," *IEEE Trans. Neural Netw. Learn. Syst.*, vol. 31, no. 4, pp. 1145–1154, Apr. 2020.

[18] B. Liu *et al.*, "Collective dynamics and control for multiple unmanned surface vessels," *IEEE Trans. Control Syst. Technol.*, vol. 28, no. 6, pp. 2540–2547, Nov. 2020.

[19] Y.-L. Wang and Q.-L. Han, "Network-based modelling and dynamic output feedback control for unmanned marine vehicles in network environments," *Automatica*, vol. 91, pp. 43–53, May 2018.

[20] Z. Peng, Y. Jiang, and J. Wang, "Event-triggered dynamic surface control of an underactuated autonomous surface vehicle for target enclosing," *IEEE Trans. Ind. Electron.*, vol. 68, no. 4, pp. 3402–3412, Apr. 2021, doi: 10.1109/TIE.2020.2978713.

[21] B.-B. Hu, H.-T. Zhang, and J. Wang, "Multiple-target surrounding and collision avoidance with second-order nonlinear multiagent systems," *IEEE Trans. Ind. Electron.*, vol. 68, no. 8, pp. 7454–7463, Aug. 2021.

[22] B. Liu, H.-T. Zhang, H. Meng, D. Fu, and H. Su, "Scanning-chain formation control for multiple unmanned surface vessels to pass through water channels," *IEEE Trans. Cybern.*, early access, Jun. 24, 2020, doi: 10.1109/TCYB.2020.2997833.

[23] Z. Peng, J. Wang, D. Wang, and Q.-L. Han, "An overview of recent advances in coordinated control of multiple autonomous surface vehicles," *IEEE Trans. Ind. Informat.*, vol. 17, no. 2, pp. 732–745, Feb. 2021, doi: 10.1109/TII.2020.3004343.

[24] B.-B. Hu, H.-T. Zhang, B. Liu, H. Meng, and G. Chen, "Distributed surrounding control of multiple unmanned surface vessels with varying interconnection topologies," *IEEE Trans. Control Syst. Technol.*, early access, May 5, 2021, doi: 10.1109/TCST.2021.3057640.

[25] B. Hu and H.-T. Zhang, "Bearing-only motional target-surrounding control for multiple unmanned surface vessels," *IEEE Trans. Ind. Electron.*, early access, May 5, 2021, doi: 10.1109/TIE.2021.3076719.

[26] J. L. Crassidis, D. J. Mook, and J. M. McGrath, "Automatic carrier landing system utilizing aircraft sensors," *J. Guid., Control, Dyn.*, vol. 16, no. 5, pp. 914–921, Sep. 1993.

[27] J. Urnes and R. Hess, "Development of the FA-18A automatic carrier landing system," *J. Guid., Control, Dyn.*, vol. 8, no. 3, pp. 289–295, 1985.

[28] J. Rife *et al.*, "Navigation, interference suppression, and fault monitoring in the sea-based joint precision approach and landing system," *Proc. IEEE*, vol. 96, no. 12, pp. 1958–1975, Dec. 2008.

[29] K. Boseley and J. Waid, "Demonstration system for using shipboard-relative GPS," *GPS World*, vol. 16, no. 4, pp. 26–33, 2005.

[30] S. Lin, M. A. Garratt, and A. J. Lambert, "Monocular vision-based real-time target recognition and tracking for autonomously landing an UAV in a cluttered shipboard environment," *Auto. Robots*, vol. 41, no. 4, pp. 881–901, Apr. 2017.

[31] H. J. Kim *et al.*, "Fully autonomous vision-based net-recovery landing system for a fixed-wing UAV," *IEEE/ASME Trans. Mechatronics*, vol. 18, no. 4, pp. 1320–1333, Aug. 2013.

[32] P. Serra, R. Cunha, T. Hamel, D. Cabecinhas, and C. Silvestre, "Landing of a quadrotor on a moving target using dynamic image-based visual servo control," *IEEE Trans. Robot.*, vol. 32, no. 6, pp. 1524–1535, Dec. 2016.

[33] M. Beul *et al.*, "Team NimbRo at MBZIRC 2017: Fast landing on a moving target and treasure hunting with a team of micro aerial vehicles," *J. Field Robot.*, vol. 36, no. 1, pp. 204–229, Jan. 2019.

[34] D. Tzoumanikas, W. Li, M. Grimm, K. Zhang, M. Kovac, and S. Leutenegger, "Fully autonomous micro air vehicle flight and landing on a moving target using visual-inertial estimation and model-predictive control," *J. Field Robot.*, vol. 36, no. 1, pp. 49–77, Jan. 2019.

[35] T. Baca *et al.*, "Autonomous landing on a moving vehicle with an unmanned aerial vehicle," *J. Field Robot.*, vol. 36, no. 5, pp. 874–891, 2019.

[36] A. Rodriguez-Ramos, C. Sampedro, H. Bavle, P. de la Puente, and P. Campoy, "A deep reinforcement learning strategy for UAV autonomous landing on a moving platform," *J. Intell. Robotic Syst.*, vol. 93, nos. 1–2, pp. 351–366, Feb. 2019.

[37] Z. Wu *et al.*, "Autonomous UAV landing system based on visual navigation," in *Proc. IEEE Int. Conf. Imag. Syst. Techn. (IST)*, Dec. 2019, pp. 1–6.

[38] S. Lee *et al.*, "Sliding mode guidance and control for UAV carrier landing," *IEEE Trans. Aerosp. Electron. Syst.*, vol. 55, no. 2, pp. 951–966, Apr. 2019.

[39] K. Xia and H. Son, "Adaptive fixed-time control of autonomous VTOL UAVs for ship landing operations," *J. Franklin Inst.*, vol. 357, no. 10, pp. 6175–6196, Jul. 2020, doi: 10.1016/j.jfranklin.2020.04.041.

[40] Y. Meng, W. Wang, H. Han, and J. Ban, "A visual/inertial integrated landing guidance method for UAV landing on the ship," *Aerosp. Sci. Technol.*, vol. 85, pp. 474–480, Feb. 2019.

[41] C. K. Tan, J. Wang, Y. C. Paw, and F. Liao, "Autonomous ship deck landing of a quadrotor using invariant ellipsoid method," *IEEE Trans. Aerosp. Electron. Syst.*, vol. 52, no. 2, pp. 891–903, Apr. 2016.

[42] Y. Meng, W. Wang, H. Han, and M. Zhang, "A vision/radar/INS integrated guidance method for shipboard landing," *IEEE Trans. Ind. Electron.*, vol. 66, no. 11, pp. 8803–8810, Nov. 2019.

[43] I. Bayezit and B. Fidan, "Distributed cohesive motion control of flight vehicle formations," *IEEE Trans. Ind. Electron.*, vol. 60, no. 12, pp. 5763–5772, Dec. 2013.

[44] A. Karimoddini, H. Lin, B. M. Chen, and T. H. Lee, "Hybrid three-dimensional formation control for unmanned helicopters," *Automatica*, vol. 49, no. 2, pp. 424–433, Feb. 2013.

[45] J. Wang and M. Xin, "Integrated optimal formation control of multiple unmanned aerial vehicles," *IEEE Trans. Control Syst. Technol.*, vol. 21, no. 5, pp. 1731–1744, Sep. 2013.

[46] X. Dong, B. Yu, Z. Shi, and Y. Zhong, "Time-varying formation control for unmanned aerial vehicles: Theories and applications," *IEEE Trans. Control Syst. Technol.*, vol. 23, no. 1, pp. 340–348, Jan. 2015.

[47] J. Huang, *Nonlinear Output Regulation: Theory and Applications*, vol. 8. Philadelphia, PA, USA: SIAM, 2004.

[48] W. L. Brogan, *Modern Control Theory*. London, U.K.: Pearson, 1991.

[49] V. Krishnamurthy and V. Seshadri, "Model reduction using the routh stability criterion," *IEEE Trans. Autom. Control*, vol. AC-23, no. 4, pp. 729–731, Aug. 1978.

This article has been accepted for inclusion in a future issue of this journal. Content is final as presented, with the exception of pagination.

ZHANG *et al.*: VISUAL NAVIGATION AND LANDING CONTROL

11

[50] J. Wang and E. Olson, "AprilTag 2: Efficient and robust fiducial detection," in *Proc. IEEE/RSJ Int. Conf. Intell. Robots Syst. (IROS)*, Oct. 2016, pp. 4193–4198.

[51] Z. Tian, C. Shen, H. Chen, and T. He, "FCOS: Fully convolutional one-stage object detection," in *Proc. IEEE/CVF Int. Conf. Comput. Vis. (ICCV)*, Oct. 2019, pp. 9627–9636.

[52] D. P. Kingma and J. Ba, "Adam: A method for stochastic optimization," 2014, *arXiv:1412.6980*. [Online]. Available: http://arxiv.org/abs/1412.6980

[53] H. Strasdat, "Local accuracy and global consistency for efficient visual SLAM," Ph.D. dissertation, Dept. Comput., Imperial College London, London, U.K., 2012.

[54] R. Gilmore, *Lie Groups, Lie Algebras, and Some of Their Applications*. Chelmsford, MA, USA: Courier Corporation, 2012.

[55] H. Che and J. Wang, "A two-timescale duplex neurodynamic approach to biconvex optimization," *IEEE Trans. Neural Netw. Learn. Syst.*, vol. 30, no. 8, pp. 2503–2514, Aug. 2019.

[56] Y. Xia, J. Wang, and W. Guo, "Two projection neural networks with reduced model complexity for nonlinear programming," *IEEE Trans. Neural Netw. Learn. Syst.*, vol. 31, no. 6, pp. 2020–2029, Jun. 2020.

[57] H. K. Khalil and J. W. Grizzle, *Nonlinear Systems*. Upper Saddle River, NJ, USA: Prentice-Hall, 2002.

[58] A. Isidori, *Nonlinear Control Systems II*. London, U.K.: Springer-Verlag, 2012.

Hai-Tao Zhang (Senior Member, IEEE) received the B.E. and Ph.D. degrees in automation and control science and technology from the University of Science and Technology of China, Hefei, China, in 2000 and 2005, respectively.

In 2007, he was a Post-Doctoral Researcher with the University of Cambridge, Cambridge, U.K. Since 2005, he has been with the Huazhong University of Science and Technology, Wuhan, China, where he was an Associate Professor from 2005 to 2010, and has been a Full Professor since 2010. He is also a Cheung Kong Young Scholar. His research interests include swarming intelligence, model predictive control, and unmanned system cooperation control.

Dr. Zhang is/was an Associate Editor of the IEEE TRANSACTION ON SYSTEMS, MAN, AND CYBERNETICS: SYSTEMS, the IEEE TRANSACTIONS ON CIRCUITS AND SYSTEMS—PART II: EXPRESS BRIEFS, ASIAN JOURNAL OF CONTROL, and the IEEE Conference on Decision and Control, and American Control Conference.

Bin-Bin Hu received the B.E. degree in electrical engineering and automation from Jiangnan University, Wuxi, China, in 2017. He is currently pursuing the Ph.D. degree in control science and technology with the Huazhong University of Science and Technology, Wuhan, China.

His research interests include multiagent systems and control of unmanned surface vehicles.

Zhecheng Xu received the B.E. degree in automation from the Beijing University of Chemical Technology, Beijing, China, in 2018. He is currently pursuing the M.E. degree in control science and technology with the Huazhong University of Science and Technology, Wuhan, China.

His research interest includes control of unmanned aerial vehicles.

Zhi Cai received the B.E. degree in automation from the Huazhong University of Science and Technology, Wuhan, China, in 2018, where he is currently pursuing the M.E. degree in control science and technology.

His research interests include embedded systems and computer vision.

Bin Liu received the B.S. degree from the Wuhan University of Technology, Wuhan, China, in 2014, and the Ph.D. degree from the Huazhong University of Science and Technology, Wuhan, in 2019.

He is currently a Post-Doctoral Researcher with the Huazhong University of Science and Technology. His research interests include multi-USV formation, unmanned surface vessel control, and model predictive control.

Xudong Wang received the B.E. degree in automation from the Wuhan University of Technology, Wuhan, China, in 2015. He is currently pursuing the Ph.D. degree in control science and technology with the Huazhong University of Science and Technology, Wuhan.

His research interests include nonlinear system identification and motion control of unmanned surface vehicles.
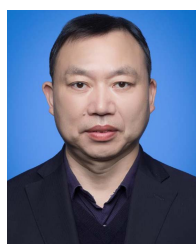
Tao Geng was born in Henan, China, in 1981. He received the Ph.D. degree in control science and engineering from the Huazhong University of Science and Technology (HUST), Wuhan, China, in 2011.

His research interests include motion planning and control of mobile robot.

Sheng Zhong received the Ph.D. degree in pattern recognition and intelligent system from the Huazhong University of Science and Technology, Wuhan, China, in 2005.

He is currently a Professor with the School of AI and Automation, Huazhong University of Science and Technology. He has undertaken a number of national research projects. His research interests are pattern recognition, image processing, and real-time embedded systems.

Jin Zhao (Senior Member, IEEE) was born in Hubei, China, in 1967. He received the B.E. and Ph.D. degrees from the Department of Control Science and Engineering, Huazhong University of Science and Technology (HUST), Wuhan, China, in 1989 and 1994, respectively.

Since 2004, he has been a Full Professor with the School of Automation, HUST. From 2001 to 2002, he was a Visiting Scholar with the Power Electronics Research Laboratory, University of Tennessee, Knoxville, TN, USA. He is currently involved in research and applications of power electronics, electrical drives, fault diagnosis, and intelligent control. He is the author or coauthor of more than 200 technical articles.